Supplementary Information

High-Capacity Sulfur Copolymer Cathode with Metallic Fibril-Based Current Collector and Conductive Capping Layer†

Dongyeeb Shin,‡[a] Yongkwon Song,‡[a] Donghyeon Nam,[a] Jun Hyuk Moon,[c] Seung Woo Lee*[d] and Jinhan Cho*[ab]

[a]*Department of Chemical and Biological Engineering, Korea University, 145 Anam-ro, Seongbuk-gu, Seoul 02841, Republic of Korea. E-mail: jinhan71@korea.ac.kr*

[b]*KU-KIST Graduate School of Converging Science and Technology, Korea University, 145 Anam-ro, Seongbuk-gu, Seoul 02841, Republic of Korea.*

[c]*Department of Chemical and Biomolecular Engineering, Sogang University, Baekbeom-ro 35, Mapo-gu, Seoul 04107, Republic of Korea.*

[d]*The George W. Woodruff School of Mechanical Engineering, Georgia Institute of Technology, Atlanta, Georgia 30332, USA. E-mail: seung.lee@me.gatech.edu*

‡These authors equally contributed to this work.

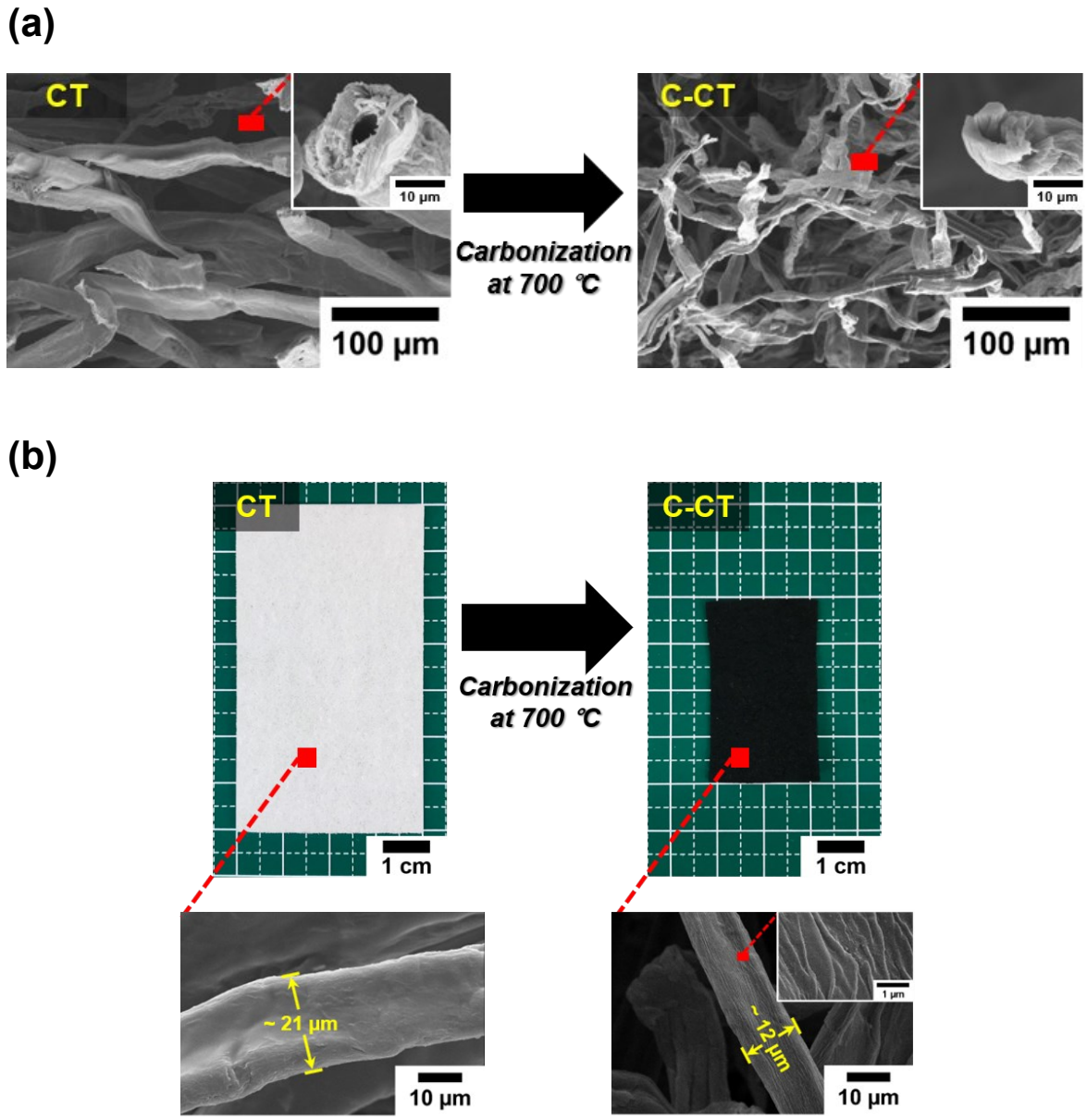

Fig. S1 (a) Cross-sectional FE-SEM images of the initial CT and C-CT carbonized at 700 °C. (b) Photographic and FE-SEM images of the CT and C-CT.

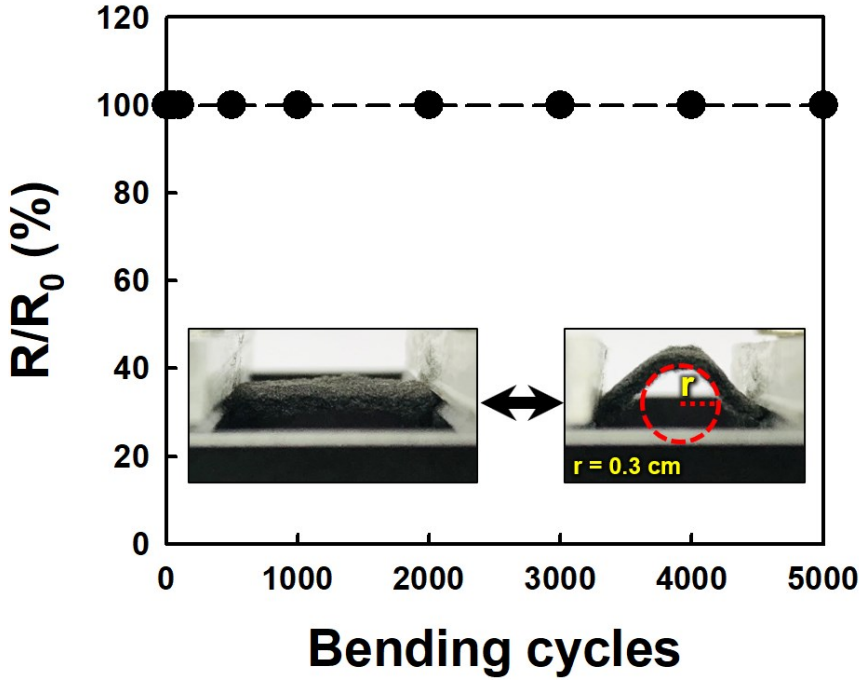

Fig. S2 Electrical stability of the C-CT as a function of bending cycling number. The resistance change (R/R_0) of the C-CT with sheet resistance of ~361 Ω sq^{-1} (R_0) at the initial (flat) state was investigated as a function of the bending cycling number. In this case, the C-CT displayed electrical stability and maintained 100 % of the initial conductivity after 5000 bending cycles (sample length = 2 cm, bending radius (r) = 0.3 cm).

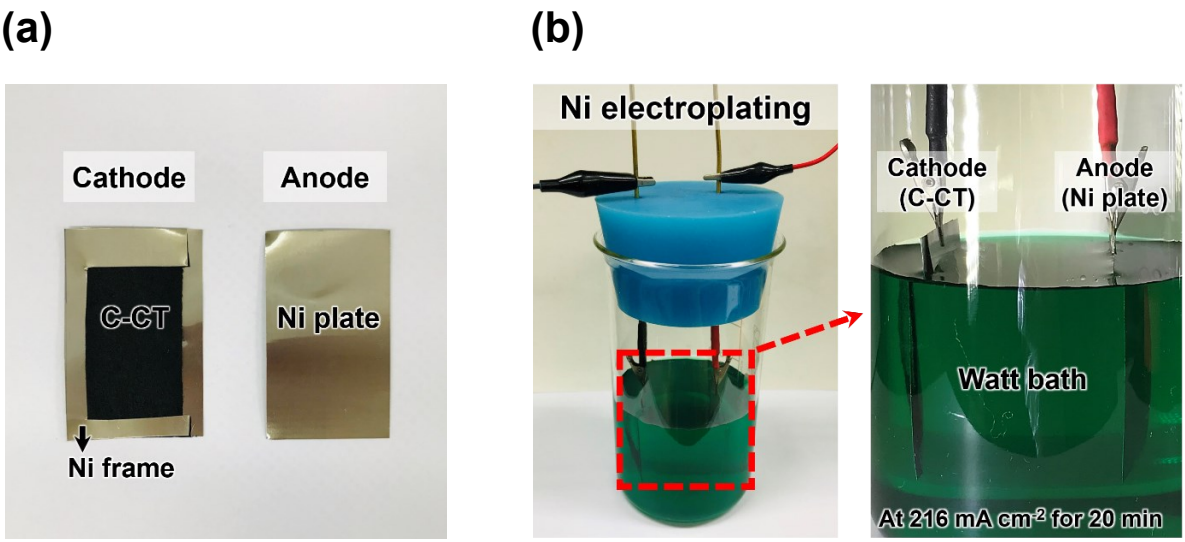

Fig. S3 (a) Photographic images of the C-CT (cathode), Ni plate (anode), and (b) two-electrode configuration-based Ni electroplating device.

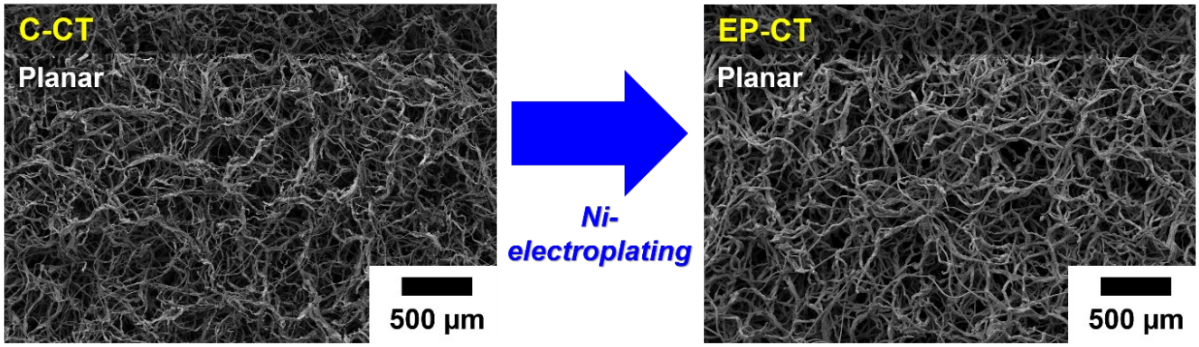

Fig. S4 FE-SEM images of the C-CT and EP-CT electroplated at a current density of 216 mA cm^{-2} for 20 min.

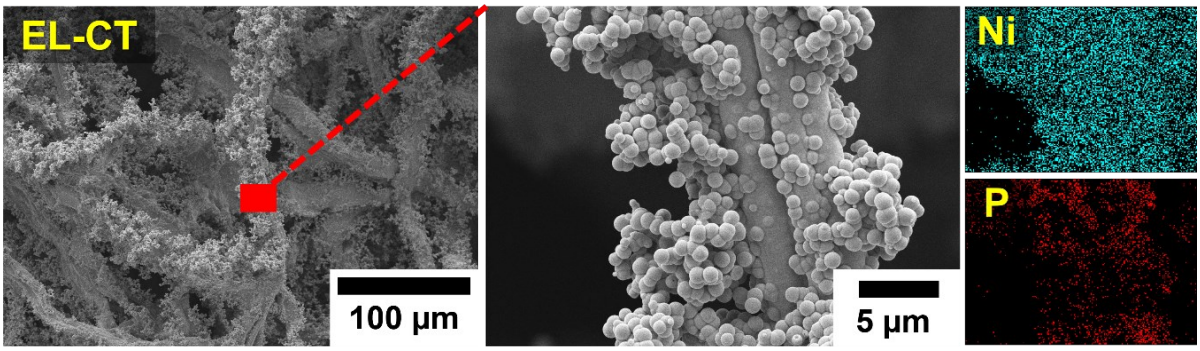

Fig. S5 FE-SEM images and EDS maps of the EL-CT. For the preparation of the EL-CT, the C-CT was first immersed into a sensitizing solution (0.05 M $SnCl_2 \cdot 2H_2O$ and 0.15 M HCl) and a $PdCl_2$ solution (0.6 mM $PdCl_2$ and 0.03 M HCl). After the C-CT was washed three times with deionized water, 45 g L^{-1} $NiSO_4 \cdot 6H_2O$, 240 g L^{-1} $NaH_2PO_2 \cdot H_2O$, 30 g L^{-1} $NaC_6H_5O_7 \cdot 2H_2O$, and 50 g L^{-1} NH_4Cl were added to the mixture, which was stirred at room temperature and adjusted to pH 9 using NH_4OH. After raising the temperature of the solution up to 80 °C, the C-CT was inserted, and stirring was applied for 120 min. After the reaction, the EL-CT was repeatedly washed with deionized water and dried (Ni loading amount: ~0.0289 g cm^{-1}). Therefore, electroless deposited Ni layer of the EL-CT included relatively large amounts of organic impurities compared to the electroplated Ni layer of the EP-CT.

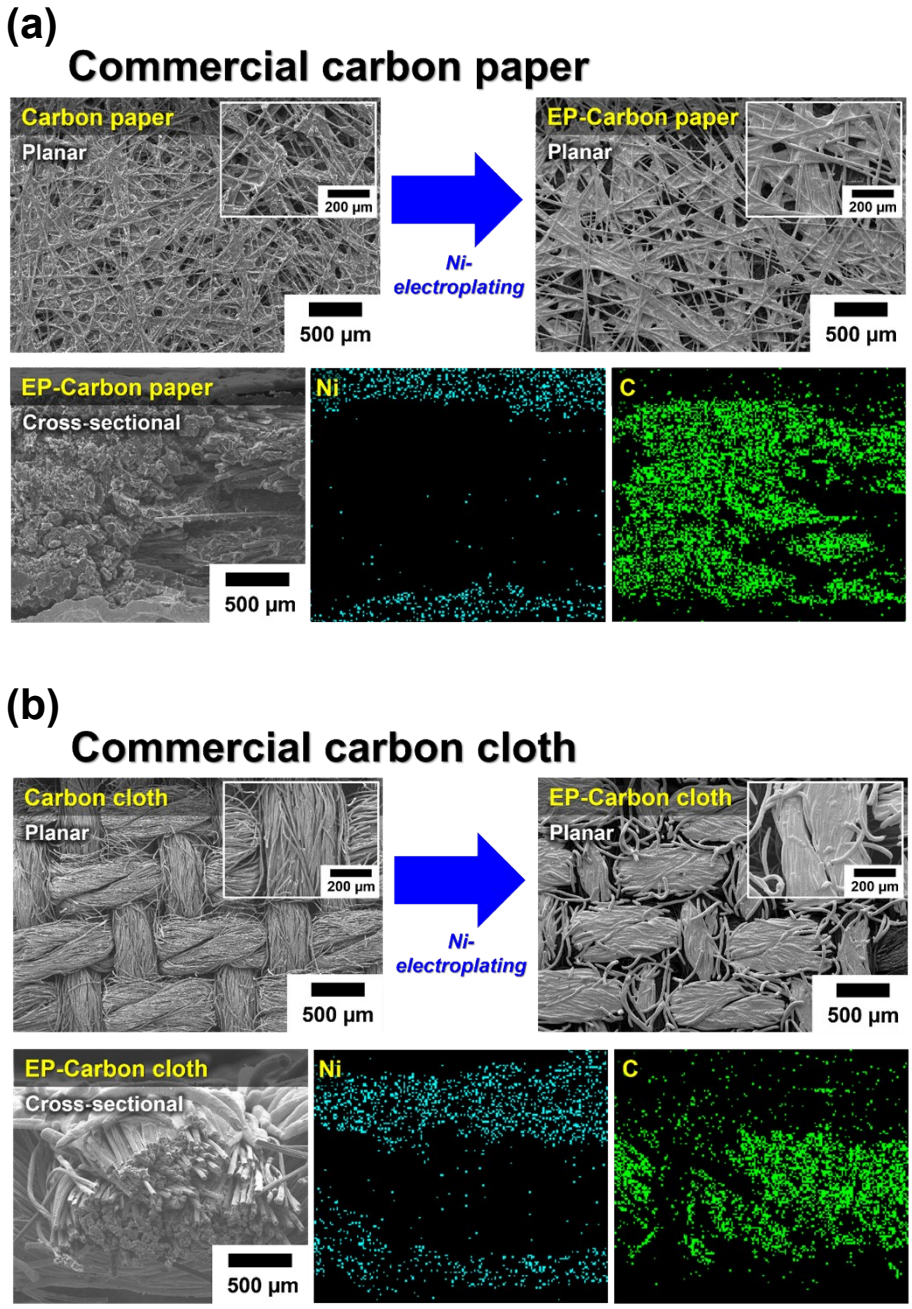

Fig. S6 FE-SEM images and EDS maps of (a) EP-carbon paper and (b) EP-carbon cloth electroplated at a current density of 216 mA cm^{-2} for 20 min. These phenomena evidently showed that the electroplated Ni layer was concentrated on the outermost surface (i.e., top and bottom surface) of carbon paper and carbon cloth because of their densely packed fibril structure and hydrophobic properties.

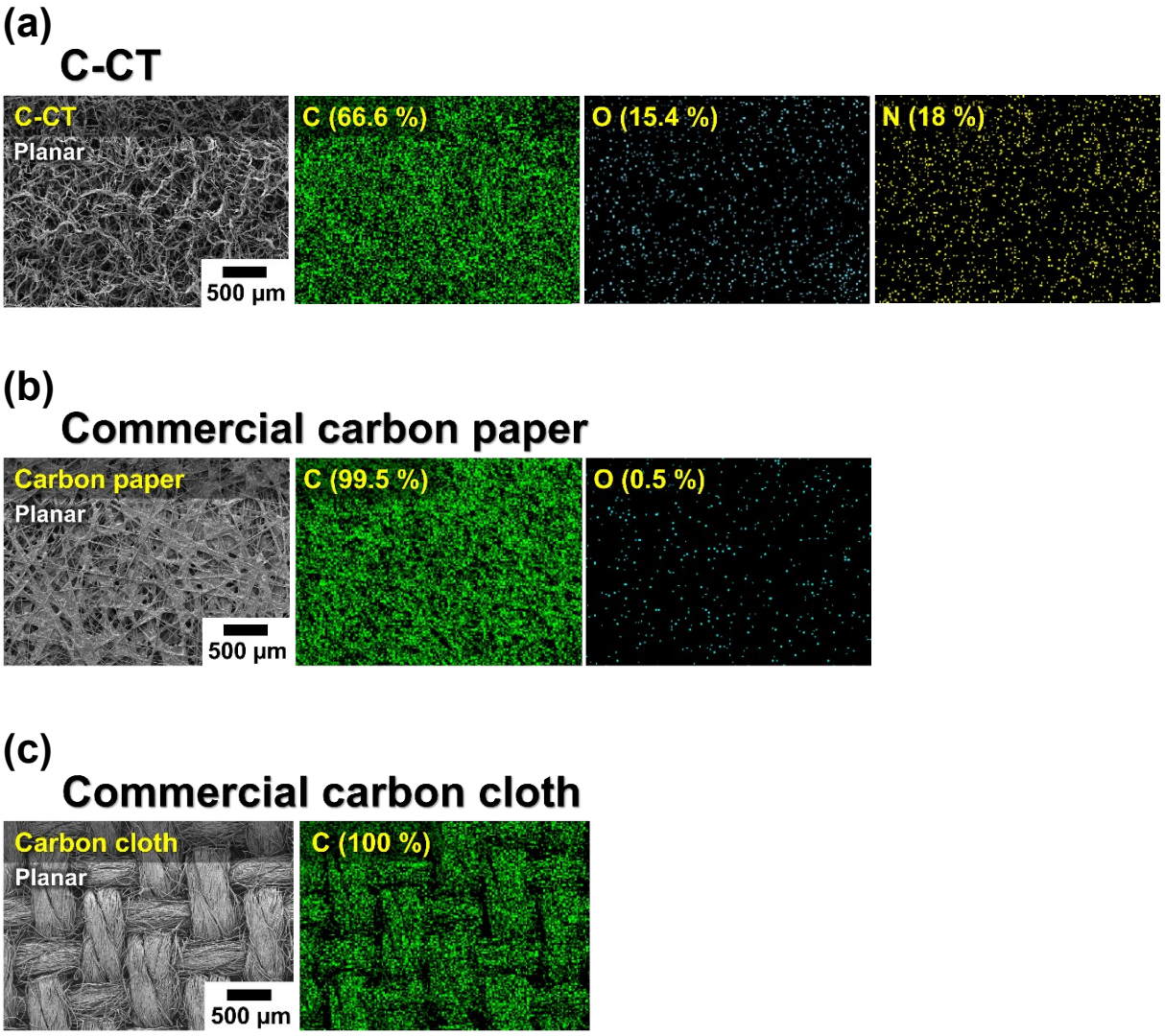

Fig. S7 Planar FE-SEM images and corresponding EDS maps for the C-CT, carbon paper, and carbon cloth. In this case, the C-CT had larger amounts of hydrophilic moieties (by the ratio of O and N atoms) compared to commercial carbon paper and carbon cloth. These results also indirectly suggest that the C-CT is highly advantageous for electrolyte infiltration.

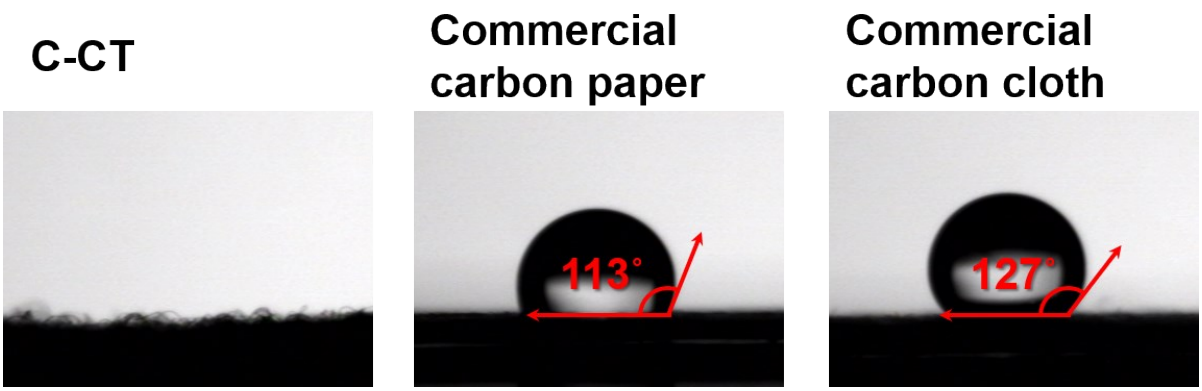

Fig. S8 Water contact angles of the C-CT, carbon paper, and carbon cloth. These results imply that the C-CT has a more advantageous hydrophilic property for electrolyte infiltration than commercial carbon paper and carbon cloth.

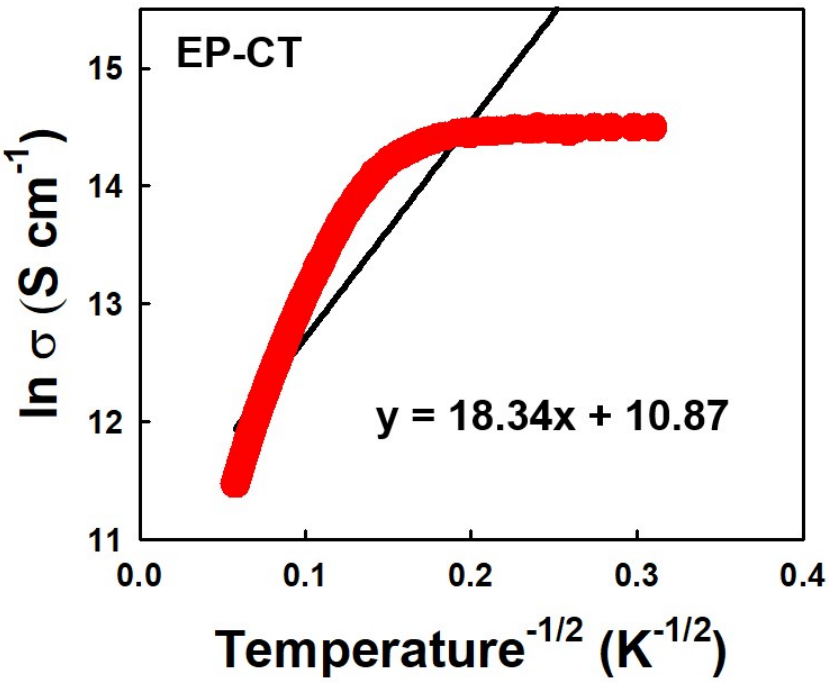

Fig. S9 Plot of ln σ vs. $T^{-1/2}$ (for tunneling) of the EP-CT. The electron transport mechanism of semiconductors can be described by the variable-range hopping or tunneling conduction mechanism as follows:

$$\sigma = \sigma_0 \exp(-A/T^{1/(d+1)})$$

where σ, *A*, T, and *d* are the electrical conductivity, constant, absolute temperature (K), and dimensionality (*d* = 3 for hopping and *d* = 1 for tunneling), respectively. The natural log electrical conductivity vs. inverse temperature plots for the EP-CT did not show a linear dependence for hopping (**Fig. 3g**) or tunneling (**Fig. S9**) mechanism, suggesting metallic conduction of the EP-CT.

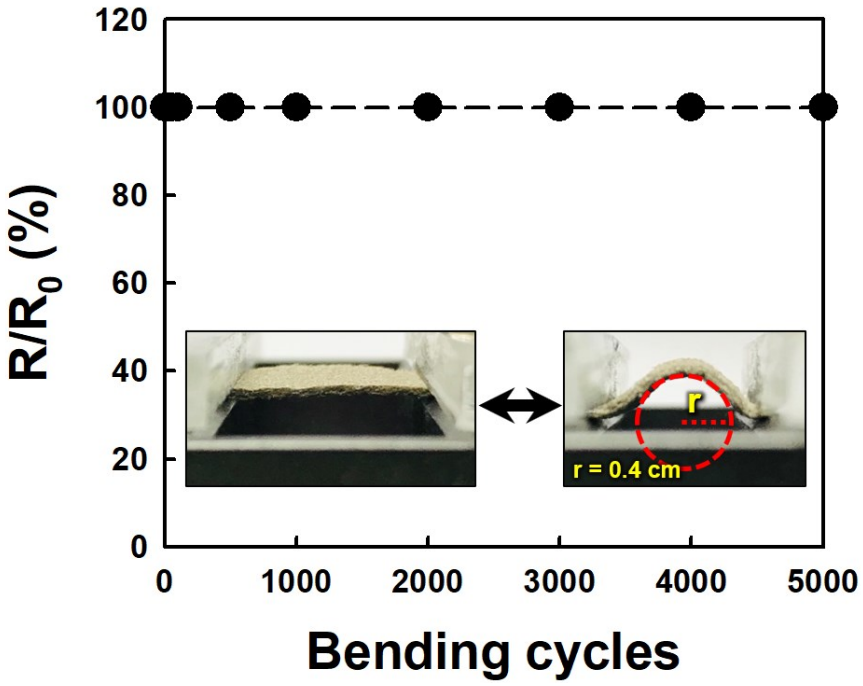

Fig. S10 Electrical stability of the EP-CT as a function of bending cycling number. The resistance change (R/R_0) of the EP-CT with sheet resistance of ~0.01 Ω sq^{-1} (R_0) at the initial (flat) state was investigated as a function of the bending cycling number. In this case, the EP-CT displayed electrical stability and maintained 100 % of the initial conductivity after 5000 bending cycles (sample length = 2 cm, bending radius (r) = 0.4 cm).

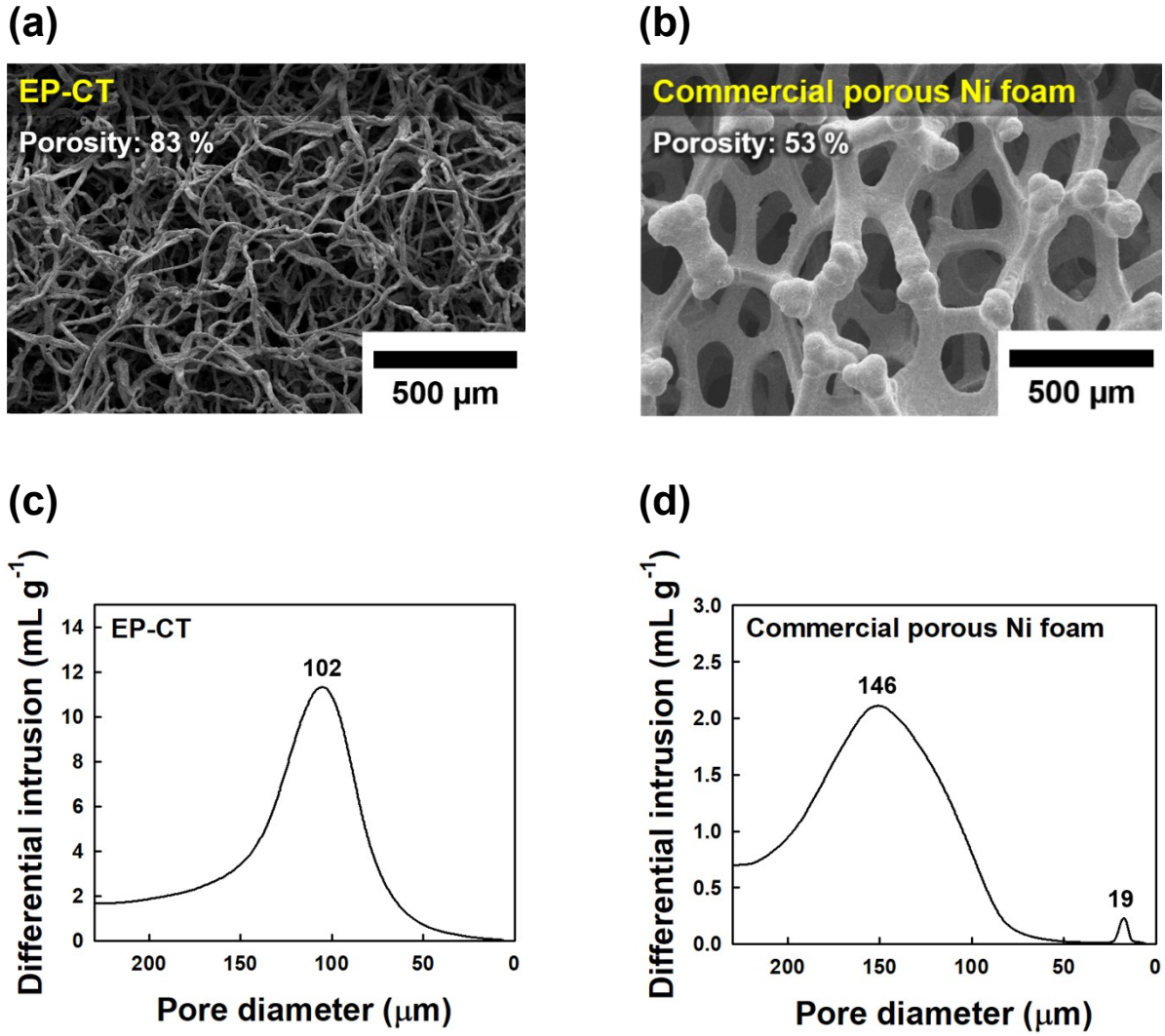

Fig. S11 FE-SEM images of the (a) EP-CT and (b) commercial porous Ni foam. Differential intrusion volume of mercury vs. pore diameter of (c) the EP-CT and (d) commercial porous Ni foam. In this case, the porosity and pore diameter were measured using mercury porosimetry technique. The pore size in the EP-CT ranged from 50 to 150 μm, with the distinct peak at 102 μm, and on the other hand, commercial porous Ni foam had the macropore size ranging from 50 to above 200 μm as well as relative small pore size from 10 to 25 μm.

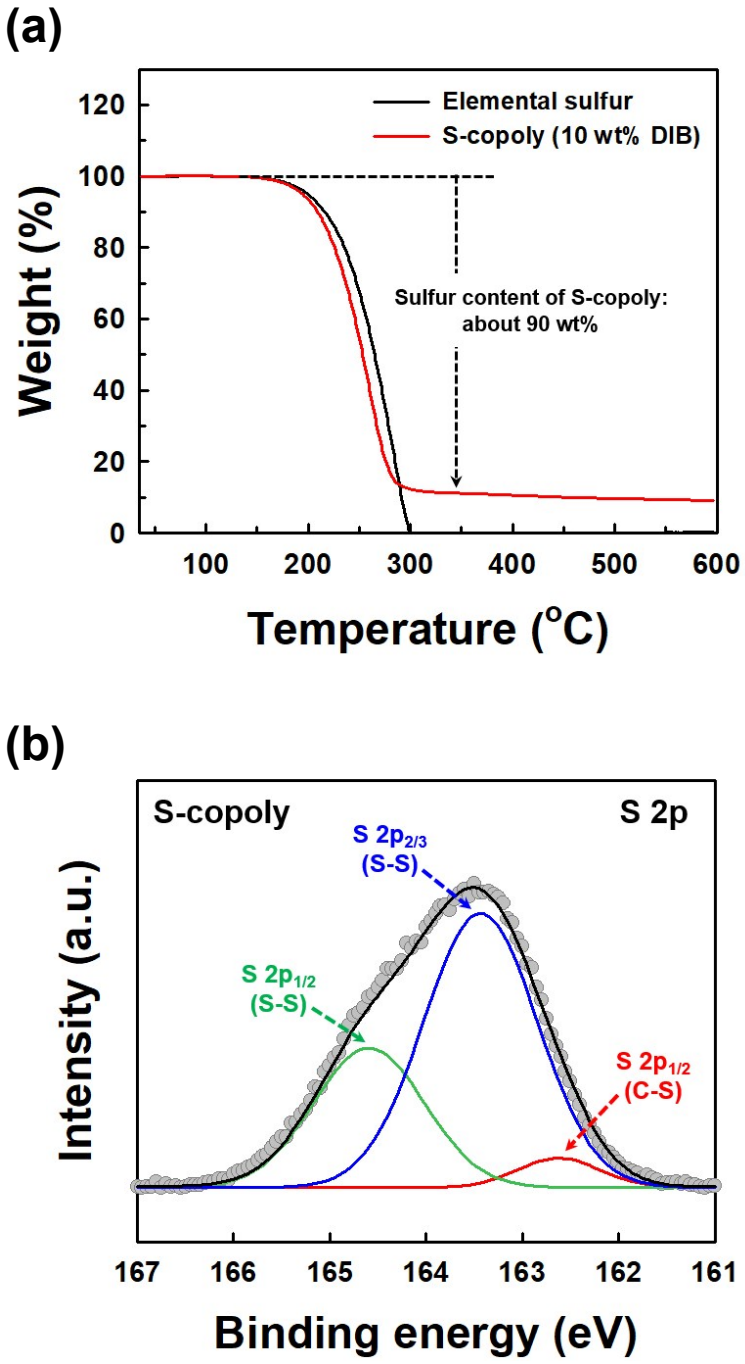

Fig. S12 (a) TGA curves with a heating rate of 5 °C min^{-1} under an argon atmosphere and (b) XPS spectra of S-copolys.

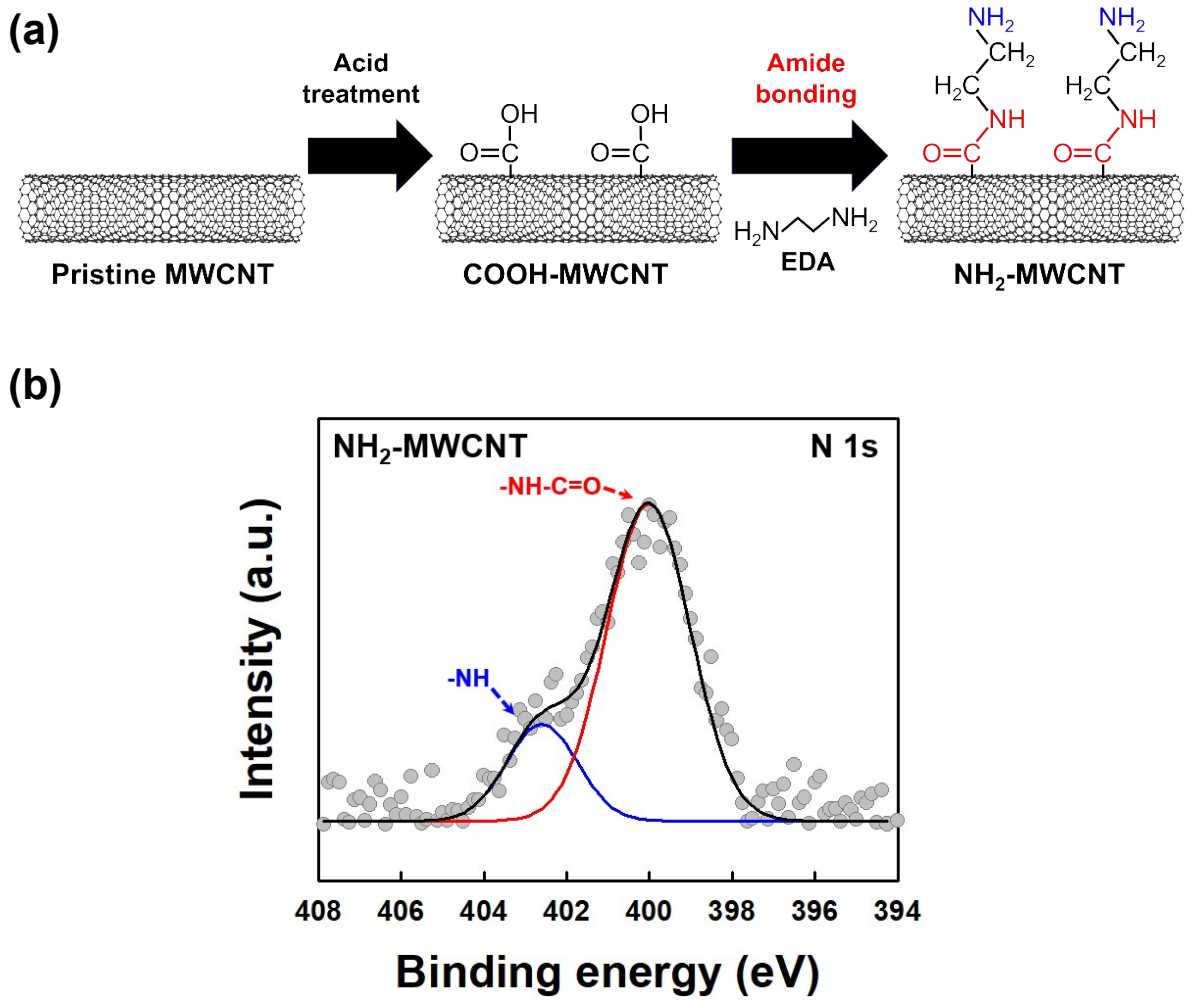

Fig. S13 (a) Schematic diagram for the preparation of NH_2-MWCNTs and (b) XPS spectra of NH_2-MWCNTs.

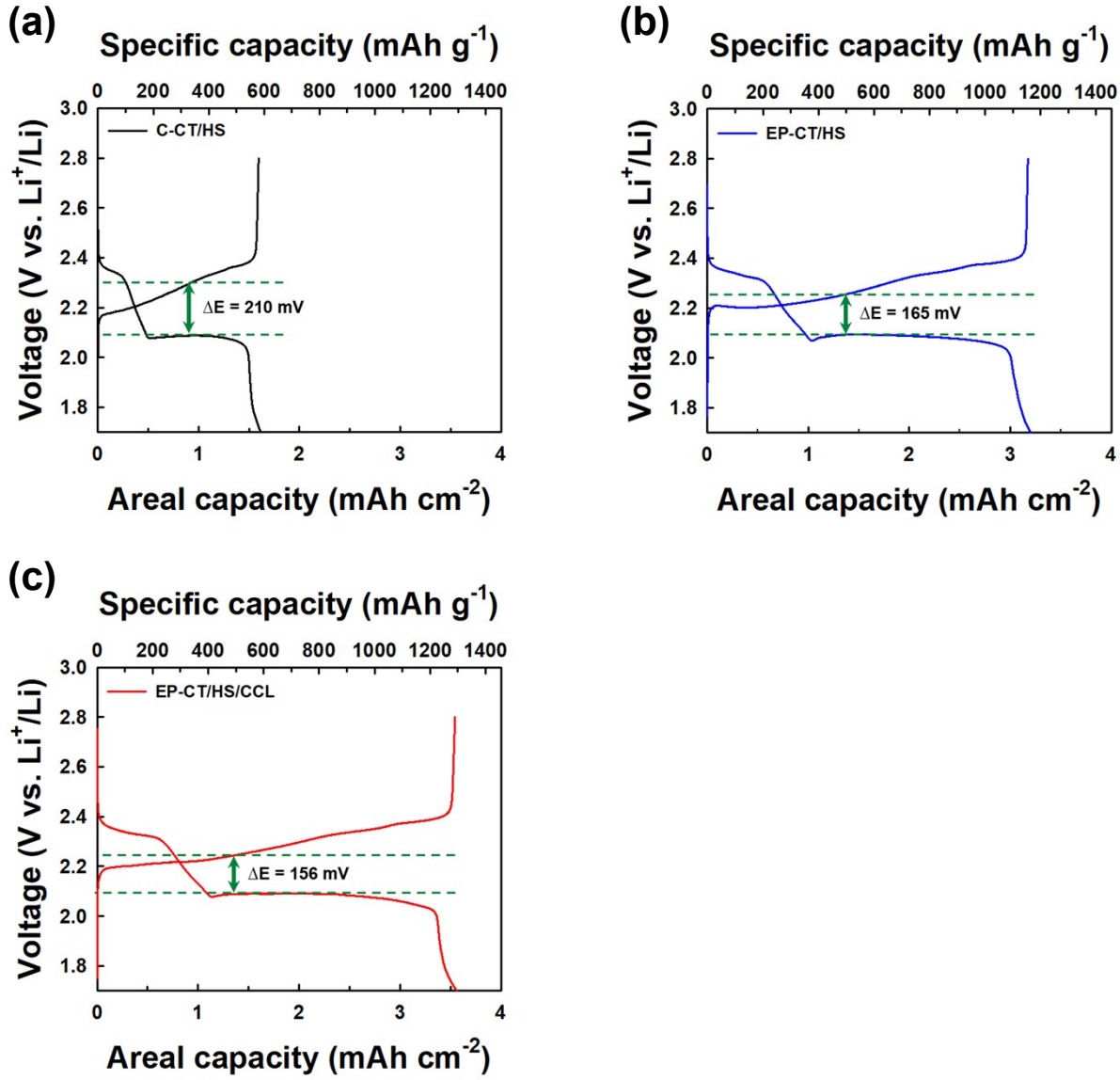

Fig. S14 Charge/discharge curves of the (a) C-CT/slurry, (b) EP-CT/slurry, and (c) EP-CT/slurry/capping layer with a S-copoly areal mass density of ~3 mg cm^{-2} at 0.1 C. Herein, the abbreviations of HS and CCL indicate (hybrid) slurry and (conductive) capping layer, respectively.

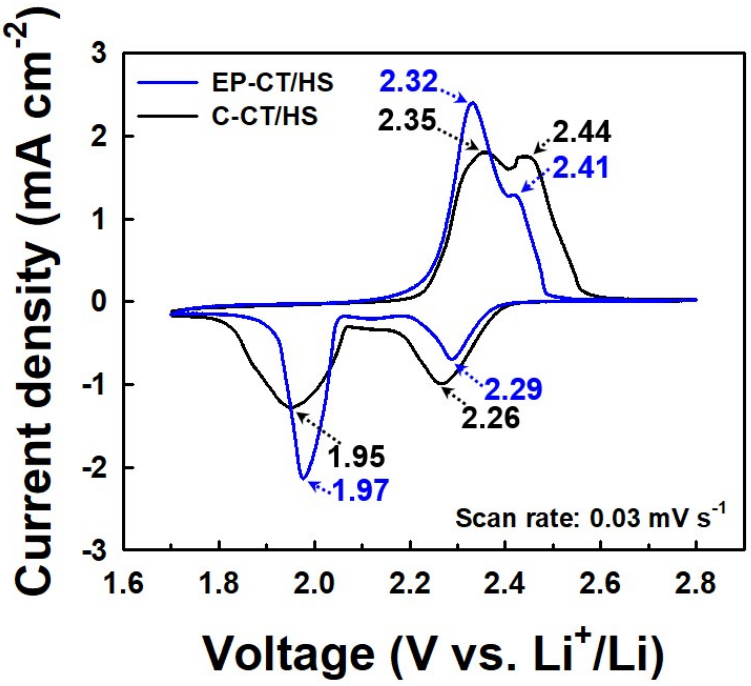

Fig. S15 CV curves of the C-CT/slurry and EP-CT/slurry at a scan rate of 0.03 mV s^{-1}. Herein, the abbreviation of HS indicates (hybrid) slurry.

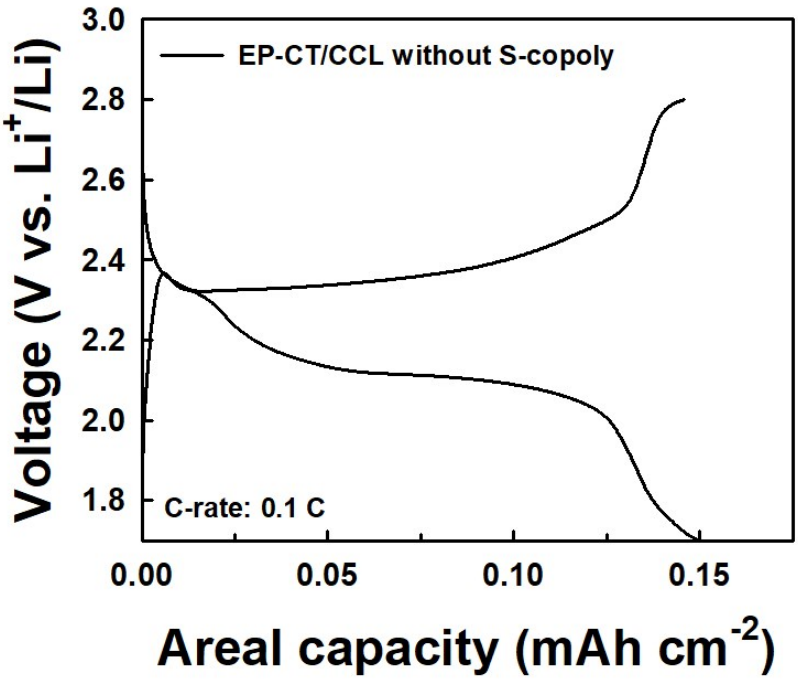

Fig. S16 Charge/discharge curve at 0.1 C of the EP-CT/capping layer without S-copolys. Herein, the abbreviation of CCL indicates (conductive) capping layer.

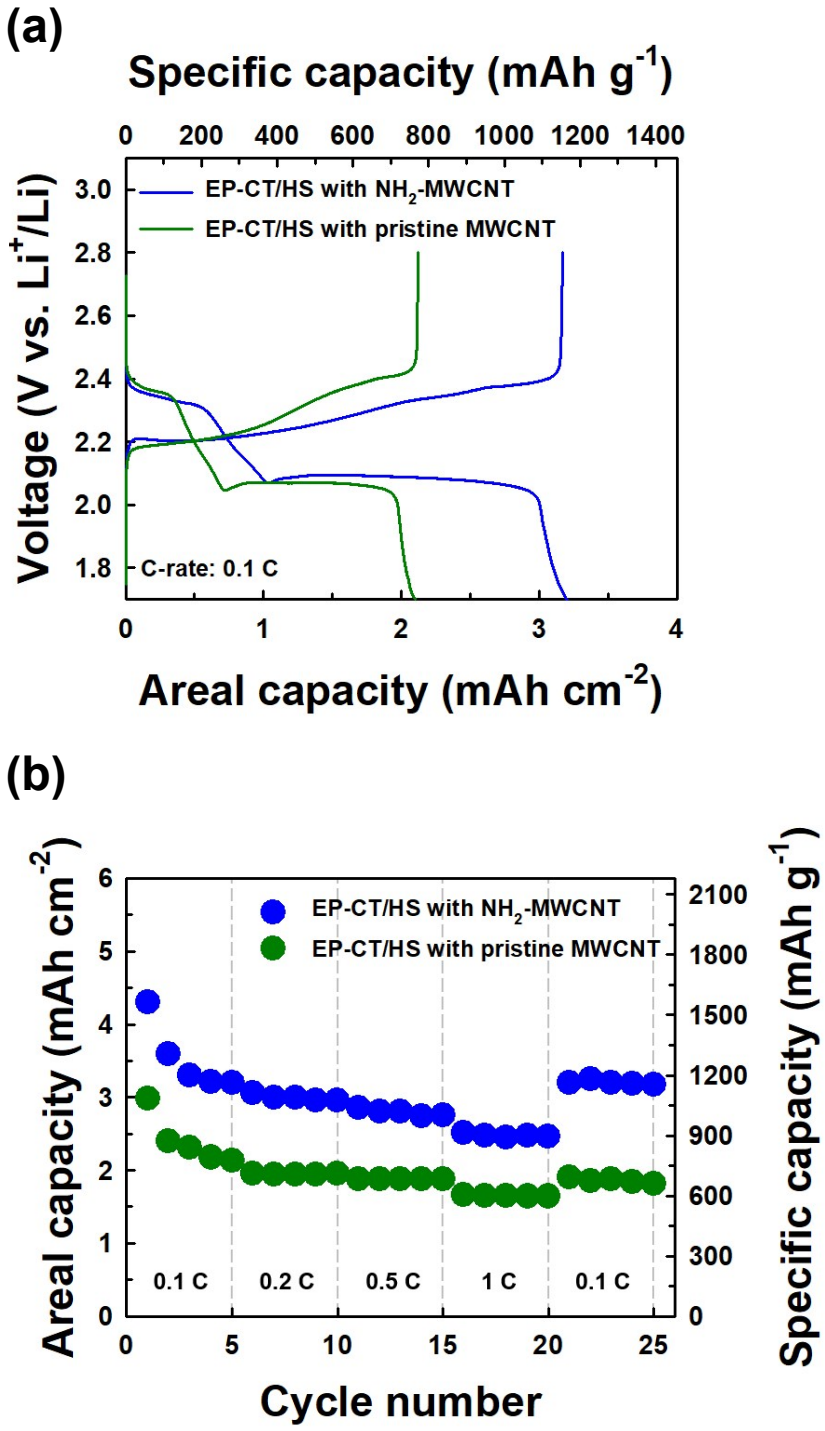

Fig. S17 (a) Charge/discharge curves at 0.1 C and (b) areal/specific capacity taken from 0.1 C to 1 C for the EP-CT/slurry with NH_2-MWCNTs and EP-CT/slurry with pristine MWCNTs. Herein, the abbreviation of HS indicates (hybrid) slurry.

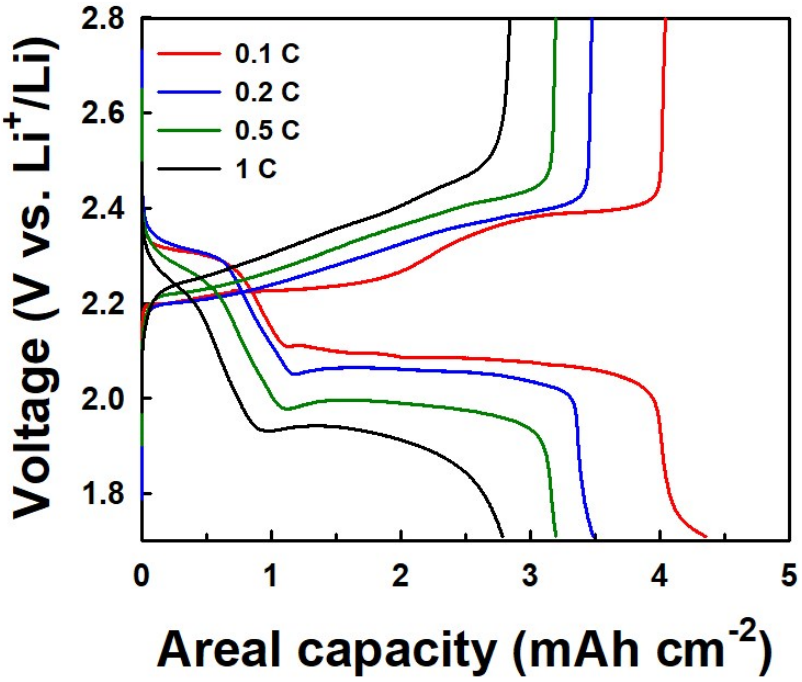

Fig. S18 Initial charge/discharge curves of the EP-CT/slurry/capping layer with a S-copoly areal mass density of ~3 mg cm^{-2} at different rates from 0.1 to 1 C.

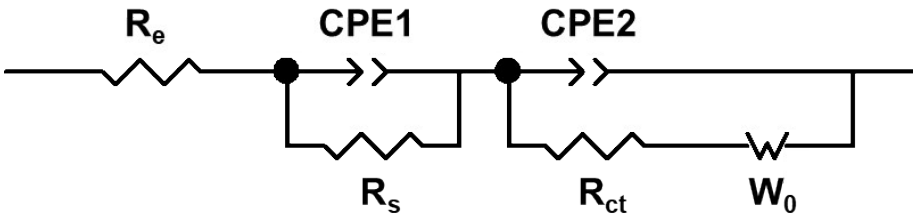

Fig. S19 Equivalent circuit for fitting the Nyquist plots of Li-S cathodes. In this circuit, the R_e, R_s, R_{ct}, and W_0 represent the impedance of electrolyte resistance, interfacial resistance (by passivation layer), charge transfer resistance, and diffusion resistance (Warburg impedance), respectively. The constant phase elements, CPE1 and CPE2, indicates the capacitance related to the interfacial layer and double-layer capacitance, respectively.

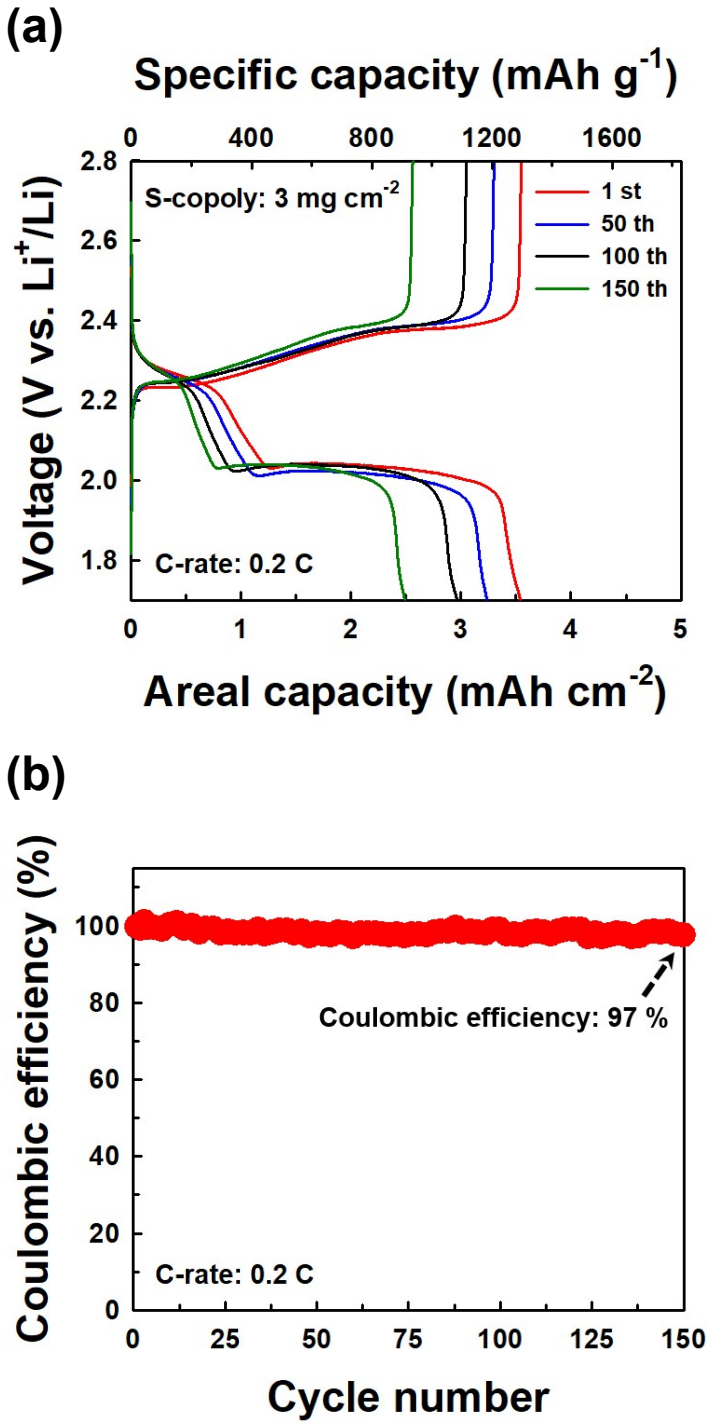

Fig. S20 (a) Charge/discharge curves and (b) Coulombic efficiency of EP-CT/slurry/capping rate with a S-copoly areal mass density of ~3 mg cm^{-2} at different cycles.

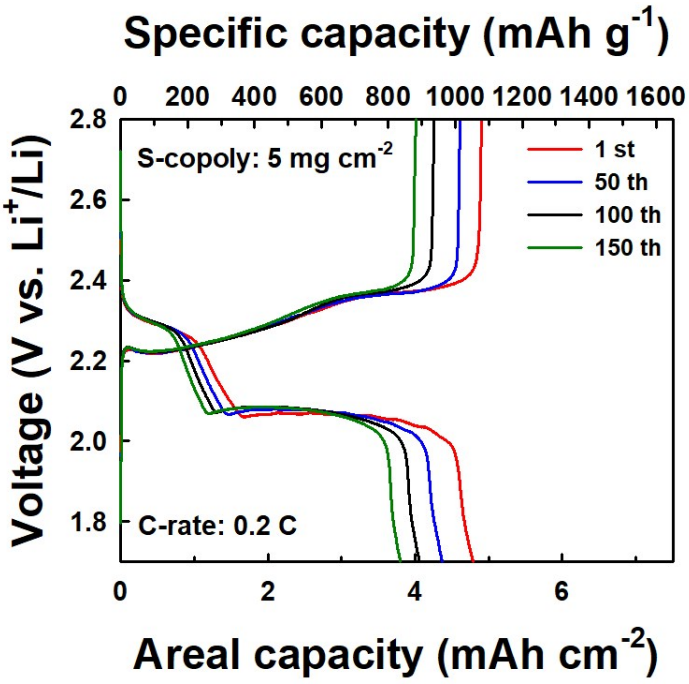

Fig. S21 Charge/discharge curves of the EP-CT/slurry/capping layer cathode with a S-copoly areal mass density of ~5 mg cm^{-2} at different cycles.

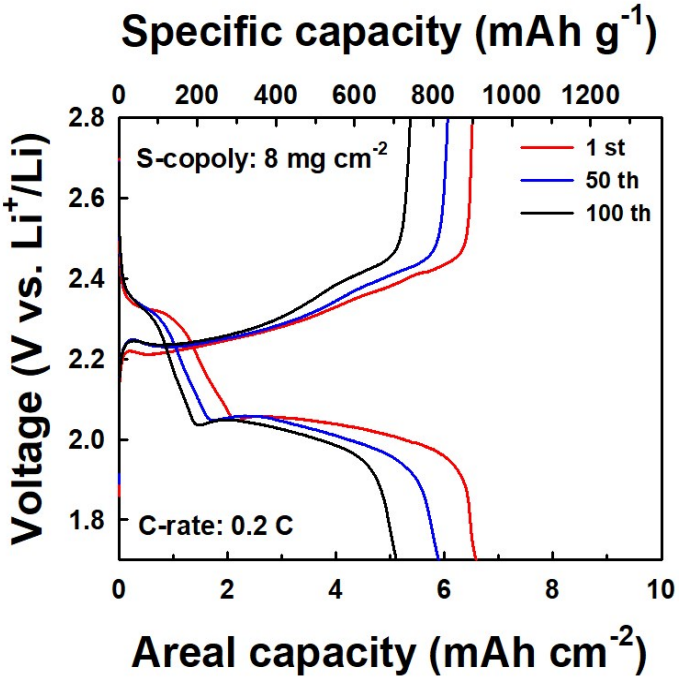

Fig. S22 Charge/discharge curves of EP-CT/slurry/capping layer with a S-copoly areal mass density of ~8 mg cm^{-2} at different cycles.

Table S1. Comparison of the performance of sulfur-based Li-S cathodes.

Cathodes	Sulfur loading (mg cm^{-2})	Areal capacity (mAh cm^{-2})	Specific capacity (mAh g^{-1})	Cycling performance		Ref.
				mAh cm^{-2}	mAh g^{-1}	
EP-CT/slurry /capping layer	2.7 (S-copolys: 3 mg cm^{-2})	4.4 @0.1 C 2.8 @1 C	1618 @0.1 C 1028 @1 C	100th, 3.0 @0.2 C	100th, 1082 @0.2 C	**Our work**
	4.5 (S-copolys: 5 mg cm^{-2})	6.1 @0.1 C 4.8 @0.2 C	1355 @0.1 C 1080 @0.2 C	150th, 3.8 @0.2 C	150th, 838 @0.2 C	
	7.2 (S-copolys: 8 mg cm^{-2})	8.3 @0.1 C 6.6 @0.2C	1149 @0.1 C 915 @0.2 C	100th, 5.1 @0.2 C	100th, 713 @0.2 C	
CF@CNTs/MgO	3.8	4.0 @0.1 C	1045 @0.1C 785 @1C	60th, 3.6 @0.1C	100th, 769 @0.2C	S1
	6.6	5.6 @0.1 C	854 @0.1C	60th, 4.8 @0.1C	60th, 730 @0.1C	
	14.4	10.4 @0.1 C	720 @0.1C	60th, 6.1 @0.1C	60th, 426 @0.1C	
CC@CoP/C-S	1.8	-	1201 @0.1C 821 @1C	-	-	S2
	4.17	-	-	-	100th, 737@0.1C	
C/SiO_2 membrane	1.5	-	1050 @0.1C 767 @1C	-	200th, 717 @0.2C	S3
	2.8	-	-	-	200th, 699 @0.2C	

CNF@VS_2/CNT@GN	5.6	6.25 @0.1C	1150 @0.1C	-	45^{th}, 685 @0.3C	S4
Ni/PCNFO-S	4.4	-	870 @0.2C 646 @1C	-	200^{th}, 391 @0.2A g^{-1}	S5
3DP-LaB_6/SP@S	4	-	1310 @0.2C 606 @1C	-	-	S6
	8.1	6.28 @0.1C	-	-	-	
	9.3	7.75 @0.05C	-	-	-	
CoP@HPCN-MWCNT/S	3.7	-	-	-	200^{th}, 729 @0.2C	S7

*CF: Carbon foam. *CC: Carbon cloth. *CNF: Carbon nanofibers. *PCNFO: Porous carbon nanofibers. *pPAN: Polyacrylonitrile.

*HPCN: Hollow polyhedral/carbon nanotube.

Table S2. Comparison of the performance of S-copoly-based Li-S cathodes.

Cathode	S-copoly loading (mg cm^{-2})	Areal capacity (mAh cm^{-2})	Specific capacity (mAh g^{-1})	Cycling performance		Ref.
				mAh cm^{-2}	mAh g^{-1}	
EP-CT/slurry /capping layer	3	4.4 @0.1 C 2.8 @1 C	1618 @0.1 C 1028 @1 C	100th, 3.0 @0.2 C	100th, 1082 @0.2 C	**Our work**
	5	6.1 @0.1 C 4.8 @0.2 C	1355 @0.1 C 1080 @0.2 C	150th, 3.8 @0.2 C	150th, 838 @0.2 C	
	8	8.3 @0.1 C 6.6 @0.2C	1149 @0.1 C 915 @0.2 C	100th, 5.1 @0.2 C	100th, 713 @0.2 C	
Al foil/ (Poly(S-*r*-DIB), Carbon, PE)	0.8	-	1100 @ 167.2 mA g^{-1}	-	100th, 823 @0.1 C	S8
Al foil/ (Poly(S-*r*-DIB), Carbon, PE)	~0.83	0.83	1225 @0.1C 800 @1C	-	100th, 1005 @0.1 C	S9
Al foil/ (S-TTCA, Super P, PVDF)	1.2	0.79	1210 @0.1 C 1090 @0.2 C	-	100th, 945 @0.2 C	S10
Al foil/ (Poly S-O-rGO, Carbon, PE)	~1.8	-	~1200 @0.1 C	100th, < 3 @0.5 C	-	S11
S-DIB@CNT membrane	1.9–2.5	-	1300 @0.1 C	-	100th, 880 @1 C	S12
Al foil/ (SBPA, Carbon, PVDF)	2.33	2.8 @0.37 mA cm^{-2}	1298 @0.1 C 632 @1 C	-	150th, 684 @0.1 C	S13
Al foil/ (cpSDG, Carbon, PVDF)	4.66	4.4@0.1C	-	100th, 2.1 @0.5C	-	S14

Carbon cloth/ (TMTD-S, KB, PVDF)	1.8	-	-	-	100^{th}, 930 @0.5 C	S15
Al foil/ (Az-S, Super P, sodium alginate)	~1.46	-	1036 @0.3 C	-	100^{th}, 515 @0.3 C	S16

*DIB: 1,3-diisopro-penylbenzene. * TTCA: Trithiocyanuric acid. *SBPA: Poly(S-*r*-DIB)-g-PANI. *cpSDG: cp(S-*r*-DIB)-Cy-rGO.

*TMTD-S: Tetramethyl thiuram disulfide-sulfur. *KB: Ketjen black. *Az-S: Azulene-based organosulfur polymer.

Notes and references

S1 M. Xiang, H. Wu, H. Liu, J. Huang, Y. Zheng, L. Yang, P. Jing, Y. Zhang, S. Dou and H. Liu, *Adv. Funct. Mater.*, 2017, **27**, 1702573.

S2 Z. Wang, J. Shen, J. Liu, X. Xu, Z. Liu, R. Hu, L. Yang, Y. Feng, J. Liu, Z. Shi, L. Ouyang, Y. Yu and M. Zhu, *Adv. Mater.*, 2019, **31**, 1902228.

S3 W. Kou, X. Li, Y. Liu, X. Zhang, S. Yang, X. Jiang, G. He, Y. Dai, W. Zheng and G. Yu, *ACS Nano*, 2019, **13**, 5900-5909.

S4 L. Wang, Y.-B. He, L. Shen, D. Lei, J. Ma, H. Ye, K. Shi, B. Li and F. Kang, *Nano Energy*, 2018, **50**, 367-375.

S5 Q. Li, J. Guo, J. Zhao, C. Wang and F. Yan, *Nanoscale*, 2019, **11**, 647-655.

S6 J. Cai, Z. Fan, J. Jin, Z. Shi, S. Dou, J. Sun and Z. Liu, *Nano Energy*, 2020, **75**, 10497.

S7 Z. Ye, Y. Jiang, J. Qian, W. Li, T. Feng, L. Li, F. Wu and R. Chen, *Nano Energy*, 2019, **64**, 103965.

S8 W. J. Chung, J. J. Griebel, E. T. Kim, H. Yoon, A. G. Simmonds, H. J. Ji, P. T. Dirlam, R. S. Glass, J. J. Wie, N. A. Nguyen, B. W. Guralnick, J. Park, Á. Somogyi, P. Theato, M. E. Mackay, Y.-E. Sung, K. Char and J. Pyun, *Nat. Chem.*, 2013, **5**, 518.

S9 A. G. Simmonds, J. J. Griebel, J. Park, K. R. Kim, W. J. Chung, V. P. Oleshko, J. Kim, E. T. Kim, R. S. Glass, C. L. Soles, Y.-E. Sung, K. Char and J. Pyun, *ACS Macro Lett.*, 2014, **3**, 229-232.

S10 H. Kim, J. Lee, H. Ahn, O. Kim and M. J. Park, *Nat. Commun.*, 2015, **6**, 7278.

S11 J. Park, E. T. Kim, C. Kim, J. Pyun, H.-S. Jang, J. Shin, J. W. Choi, K. Char and Y.-E. Sung, *Adv. Energy Mater.*, 2017, **7**, 1700074.

S12 G. Hu, Z. Sun, C. Shi, R. Fang, J. Chen, P. Hou, C. Liu, H.-M. Cheng and F. Li, *Adv. Mater.*, 2017, **29**, 1603835.

S13 J. Key, Y. Feng, J. Shen, P. Wang, H. Wang, H. Liang, R. Wang and S. Ji, *J. Electrochem. Soc.*, 2020, **167**, 020530.

S14 J. Shen, Y. Feng, P. Wang, G. Qiu, L. Zhang, L. Lu, H. Wang, R. Wang, V. Linkov and

S. Ji, *ACS Sustainable Chem. Eng.*, 2020, **8**, 10389-10401.

S15 H. Xu, Y. Shi, S. Yang and B. Li, *J. Power Sources*, 2019, **430**, 210-217.

S16 Z. Chen, J. Droste, G. Zhai, J. Zhu, J. Yang, M. R. Hansen and X. Zhuang, *Chem. Commun.*, 2019, **55**, 9047.